13th World Conference on Earthquake Engineering
Vancouver, B.C., Canada
August 1-6, 2004
Paper No. 832

DYNAMIC MODELING OF DIP-SLIP FAULTS FOR STUDYING GROUND SURFACE DEFORMATION USING APPLIED ELEMENT METHOD

Pradeep Kumar RAMANCHARLA [1], Tagel-Din HATEM [2] and Kimiro MEGURO [3]

SUMMARY

When an active bedrock fault ruptures, the movement along the fault propagates through the overlying soil and produces zones of intense shear. If the fault movement propagates upto or near the ground surface, the damage to constructed facilities due to faulting, in conjunction with that induced by strong ground motion, can be significant. This paper contributes to the understanding of the response of soil deposits to the underlying bedrock fault displacement. In the conventional attenuation relationship, peak ground acceleration shows maximum value at the closest distance from the fault. However, in the real observations, sometimes it is found that the damage near to the surface fault is not maximum, instead it is high little away from the surface rupture zone. To understand the above-mentioned response of soil deposits, we attempted to develop a new application to Applied Element Method (AEM) by modeling the fault rupture zone. In this, we study the behavior of dip-slip faults. The effect of the slip velocity on the ground motion is studied first and then the attenuation of PGA in the near fault zone is studied. Effect of the material properties is also discussed.

INTRODUCTION

Over the past few decades, significant effort has been devoted to understanding the problem of ground shaking. Accordingly, numerous design and construction procedures have been developed to minimize damage due to strong ground motion. However, the efforts towards improving our understanding of the problem of surface faulting have been relatively modest. The common practice with important facilities such as dams, nuclear power plants, and public buildings has been to avoid construction across the recognized trace of an active fault. However, in case of the buried faults our ability to delineate the possible potential hazard that can be caused due to the future rupture activity is far from complete. But, the occurrence of the catastrophic earthquakes i.e. Kocaeli, Turkey, Chi-Chi, Taiwan and etc., in the

[1] Assistant Professor, Computer Aided Structural Engineering, International Institute of Information Technology, Gachibowli, Hyderabad 500 019, India, e-mail: ramancharla@iiit.net
[2] Assistant Professor, Cairo University, Egypt, e-mail: tageldin@yahoo.com
[3] Associate Professor, IIS, University of Tokyo, 4-6-1 Komaba Meguro-ku 1538505, Japan, e-mail: meguro@iis.u-tokyo.ac.jp

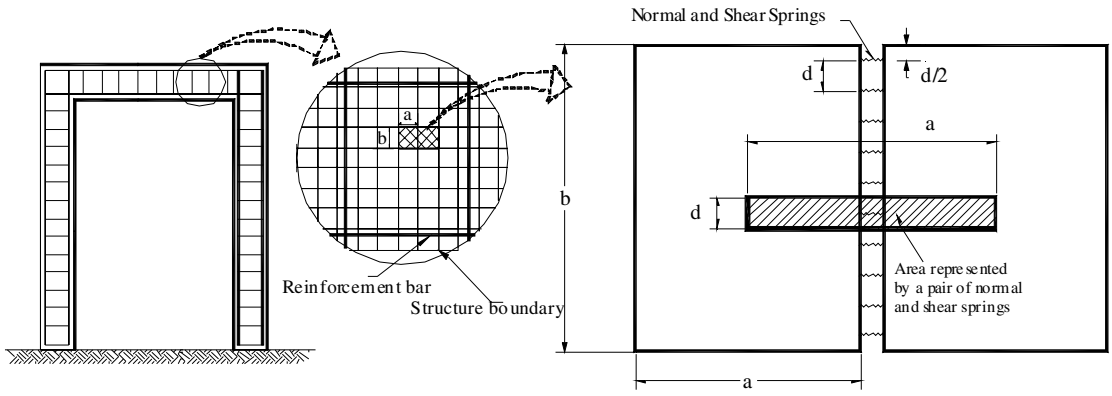

(a) Element generation for AEM

(b) Spring distribution and area of influence of each pair of springs

Fig. 1 Modelling of structure in AEM

recent times has posed many new challenges to the engineering community. Therefore, the engineering profession should develop techniques to mitigate the damaging effects of surface faulting.

Two enormously disastrous earthquakes occurred during the year 1999. The first one was an earthquake of magnitude 7.4 (Mw) occurred in Turkey on 17th August 1999 [1], and immediately following that, another event of magnitude 7.3 (Mw, Central Weather Bureau, Taiwan) occurred in Taiwan on 21st September 1999 [2]. The earthquake fault (North Anatolian Fault) in Turkey was traced over 100 km. The magnitude of right lateral movement of the fault on the ground surface was measured to be 2 to 4 m. And in Taiwan, severer effects were observed. The earthquake fault (Cher-Lung-Pu Fault) was traced for about 80 km, here the fault movement directly caused severe damage. The magnitude of maximum vertical differential movement was measured to be nearly 10.0 m. From the above two events, it is clear that the severe damage can be caused not only by the strong ground motion but also due to large surface deformations lying directly over the seismic faults. Hence, it is necessary to direct our efforts to study the relation between seismic fault characteristics, thickness of soil deposit and surface deformation.

Many researchers conducted experiments to understand the phenomena of surface failure, Cole and Lade [3] have tried to determine the location of surface fault rupture and width of the affected zone in alluvium over dip-slip fault using fault test box. They hypothesized that the results may be applicable to cohesive materials. Lade et al. [4] studied to determine the multiple failure surfaces by conducting the experiments on sand using fault test box. The results of the sand box model tests concluded that the observed displacement fields were largely the same for the different materials. Onizuka et al. [5] have modelled the deformation of ground using aluminum rods. Through experiments, they investigated bedrock stresses induced by reverse dip-slip faults. Bray [6] investigated the pattern of ruptures in clay models under 1-g subjected to dip-slip faulting. The range of bedrock's dip angle varied from 60^0 to 90^0 for both normal and reverse faults. Tani et al. [7] conducted a 1-g model study of dip-slip faulting using dry Toyoura sand as model material. Results from their first series of tests indicated that the base offset necessary for the rupture to propogate to the ground surface varied with fault orientation. These observations are in agreement with those from the study of Cole and Lade [3].

Using the above experimental methods, we can find the affected length on the surface. However, replicating the actual field conditions using experiments is very difficult, especially, controlling the

material properties and modelling the boundary conditions. Moreover, large amount of data is necessary to establish a relationship between seismic fault parameters and resulting surface deformation. On the other hand, studying this phenomenon using numerical model has the advantage of controlling the parameters like material properties, size of the model, boundary condition, dip angle, etc. Numerical model allow us to investigate a number of aspects of the fault rupture propagation phenomenon, which are difficult to study from the examination of case histories or the conduct of physical model tests. It allows for the precise control and the model used to represent the behaviour of the soil and the imposed boundary conditions. Of course, the accuracy and reliability of any numerical approach depends on the validity of the mathematical conceptualisation of the critical aspects of the problem. If the limitations of the assumptions imposed in the problem definition are understood, the numerical analyses can assist the engineer in attempting to understand the problem in question.

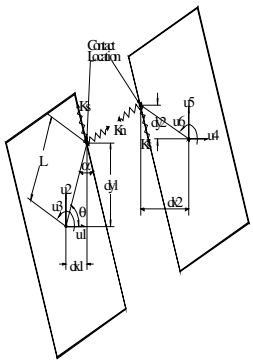

Fig. 2 Spring connectivity

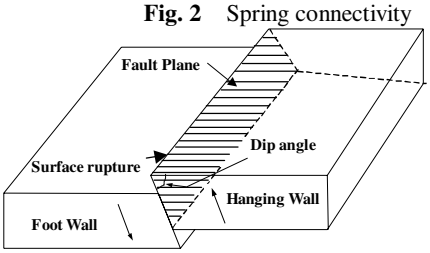

Fig. 3 Fault terminology

The discrete element approach intuitively looks promising. A soil mass is not a continuum. Instead, it is an assemblage of finite-sized particles. Inter-particle forces fundamentally determine the observed macroscopic behaviour of soil. Moreover, once a shear or tension cracks develops within the soil mass it typically becomes difficult to reliable apply a numerical approach based on the principles of continuum mechanics. The EDEM, however has a serious drawback in that it requires an enormous amount of calculation time because explicit numerical integration is unstable unless the time step used is very short (Hakuno and Meguro [8]).

APPLIED ELEMENT METHOD (AEM)

With the AEM [9~11], structure is modelled as an assembly of small elements that are made by dividing of the structure virtually, as shown in Fig. 1 (a). The two elements shown in Fig. 1(b) are assumed to be connected by pairs of normal and shear springs located at contact locations that are distributed around the element edges. Each pair of springs totally represents stresses and deformations of a certain area (hatched area in Fig. 1 (b)) of the studied elements. The spring stiffness is determined as shown in Eq. (1):

$$K_n = \frac{E \times d \times T}{a} \quad \text{and} \quad K_s = \frac{G \times d \times T}{a} \qquad (1)$$

where, d is the distance between springs, T is the thickness of the element and "a" is the length of the representative area, E and G are the Young's and shear modulus of the material, respectively. The above equation indicates that each spring represents the stiffness of an area (d x T) with length "a" of the studied material. In case of reinforcement, this area is replaced by that of the reinforcement bar. The above equation indicates that the spring stiffness is calculated as if the spring connects the element centerlines.

In 2D AEM, three degrees of freedom are assumed for each element. These degrees of freedom represent the rigid body motion of the element. Although the element motion is a rigid body motion, its internal stresses and deformations can be calculated by the spring deformation around each element. This means that although the element shape doesn't change during analysis, the behavior of assembly of elements is deformable.

$$\left[\begin{array}{c|c|c} \begin{array}{l}\mathrm{Sin}^2(\theta+\alpha)K_n \\ +\mathrm{Cos}^2(\theta+\alpha)K_s\end{array} & \begin{array}{l}-K_n\mathrm{Sin}(\theta+\alpha)\mathrm{Cos}(\theta+\alpha) \\ +K_s\mathrm{Sin}(\theta+\alpha)\mathrm{Cos}(\theta+\alpha)\end{array} & \begin{array}{l}\mathrm{Cos}(\theta+\alpha)K_sL\mathrm{Sin}(\alpha) \\ -\mathrm{Sin}(\theta+\alpha)K_nL\mathrm{Cos}(\alpha)\end{array} \\ \hline \begin{array}{l}-K_n\mathrm{Sin}(\theta+\alpha)\mathrm{Cos}(\theta+\alpha) \\ +K_s\mathrm{Sin}(\theta+\alpha)\mathrm{Cos}(\theta+\alpha)\end{array} & \begin{array}{l}\mathrm{Sin}^2(\theta+\alpha)K_s \\ +\mathrm{Cos}^2(\theta+\alpha)K_n\end{array} & \begin{array}{l}\mathrm{Cos}(\theta+\alpha)K_nL\mathrm{Cos}(\alpha) \\ +\mathrm{Sin}(\theta+\alpha)K_sL\mathrm{Sin}(\alpha)\end{array} \\ \hline \begin{array}{l}\mathrm{Cos}(\theta+\alpha)K_sL\mathrm{Sin}(\alpha) \\ -\mathrm{Sin}(\theta+\alpha)K_nL\mathrm{Cos}(\alpha)\end{array} & \begin{array}{l}\mathrm{Cos}(\theta+\alpha)K_nL\mathrm{Cos}(\alpha) \\ +\mathrm{Sin}(\theta+\alpha)K_sL\mathrm{Sin}(\alpha)\end{array} & \begin{array}{l}L^2\mathrm{Cos}^2(\alpha)K_n \\ +L^2\mathrm{Sin}^2(\alpha)K_s\end{array} \end{array}\right] \quad (2)$$

The two elements shown in Fig. 2 are assumed to be connected by only one pair of normal (stiffness: Kn) and shear (stiffness: Ks) springs. The values of (dx and dy) correspond to the relative coordinate of the contact point with respect to the centroid. To have a general stiffness matrix, the location of element and contact springs are assumed in a general position. The stiffness matrix components corresponding to each degree of freedom are determined by assuming a unit displacement in the studied direction and by determining forces at the centroid of each element. The element stiffness matrix size is only (6 x 6). Equation (2) shows the components of the upper left quarter of the stiffness matrix. All used notations in this equation are shown in Fig. 2. It is clear that the stiffness matrix depends on the contact spring stiffness and the spring location.

The stiffness matrix in Eq. (2) is for only one pair of contact springs. However, the global stiffness matrix is determined by summing up the stiffness matrices of individual pair of springs around each element. Consequently, the developed stiffness matrix is an average stiffness matrix for the element according to the stress situation around the element. This technique can be used both in load and displacement control cases. The governing equation is

$$[K_G][\Delta] = [F] \quad (3)$$

where, [KG] is the global stiffness matrix; [?] the displacement vector and [F] the applied load vector. In load control case, the vector, [F], is known before the analysis. In displacement control case, the load is applied by unit virtual displacement for one or more degrees of freedom. By using the advantage of AEM's simplicity in formulation and accuracy in non-linear range, fault rupture zone shown in Fig. 3 is modelled.

MODEL PREPARATION

The mechanism shown in **Fig. 3** is called Reverse Dip-Slip Faulting. This is one of the types of fault where the hanging wall moves upward relative to the footwall. If the direction of the movement of the hanging wall is downward then it is called normal faulting. To analyse the mechanism of fault rupture zone near dip-slip faults, the numerical model shown in **Fig. 4** is prepared. Length of the model is assumed as 1 km and depth is 150 m. The location of the base fault is assumed to lie exactly at the centre of the model.

Generally, soil strata and bedrock extend upto tens of kilometres in horizontal direction. Numerical modelling of such a large media is a difficult task and moreover, for studying the surface behavior near the active fault region, it is necessary to model the small portion of the region that includes all the effects when the bedrock moves. For studying the selected region numerically, we assumed the boundary on left side to be fixed in horizontal direction. In order to avoid the interference of boundary condition on numerical results, left side boundary is kept at sufficient distance from the fault zone. The Bottom of the bedrock is assumed as fixed.

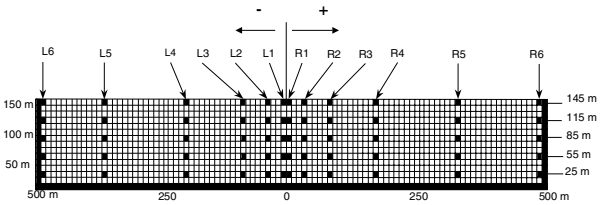

Fig. 4 Numerical model for fault rupture study

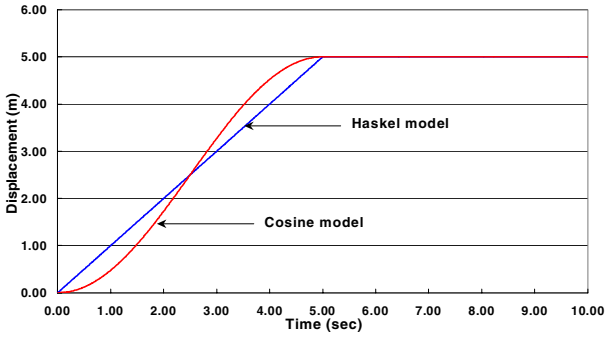

Fig. 5 Slip function

When the model is set with no loading except the self-weight, which is applied as gravity load, the model exhibits free vibrations across the equilibrium position. These vibrations will decay consuming the large amount of CPU time. Hence, the static analysis is performed first and the self-weight is applied in increments. After the total self-weight is applied in static way, the model for performing dynamic fault rupture analysis is ready.

SLIP RATE OF FAULT

After setting the model to perform dynamic analysis, it is necessary to know the influence of the slip rate of the fault on the vibration. The slip rate of the fault is one of the five source parameters that are important for discussion while dealing with the dynamic characteristics of fault rupture propagation. These parameters are; the fault length (L), the fault width (W), rupture velocity (V_R), the final offset (D), and rise time (t). Since we are dealing with 2D model, length of the fault is not considered and width of the fault is kept constant in all the cases of analysis. The remaining three parameters are observed varying their values. Slip velocity is dependent on the last two parameters i.e. final offset (D) and rise time (t).

To understand the effect of slip rate, linear elastic analyses were first performed. Two kinds of slip functions as shown in **Fig. 5** were observed. First, the ramp model [12, 13] is observed and later cosine model is used in the analysis. Figure 6 (a) shows the horizontal and vertical displacement time history of the element "R5" on the hanging wall, **Fig. 6 (b)** is showing the kinetic and potential energy changes in the system and **Figs. 6 (c)** and **(d)** show the horizontal and vertical velocity time histories of element "R5" on hanging wall and element "L5" on footwall, respectively. From the set of figures, it can easily seen that the effect of input base displacement is affecting the vibration, especially from **Fig. 6 (c)** sudden rise and drop in the velocity exactly at the starting and ending of the constant rate displacement. The reason for this behavior is due the input displacement function, which has sudden rise at the start of input and constant velocity till 5 seconds and then sudden drop at 5 sec. Hence, to remove this effect, the input base displacement following Cosine model is considered (see **Fig. 5**). Set of **Figs. 7 (a) ~ (d)** are showing the similar results as discussed in the previous paragraph. From this, it can be easily seen that there is no effect of input base displacement.

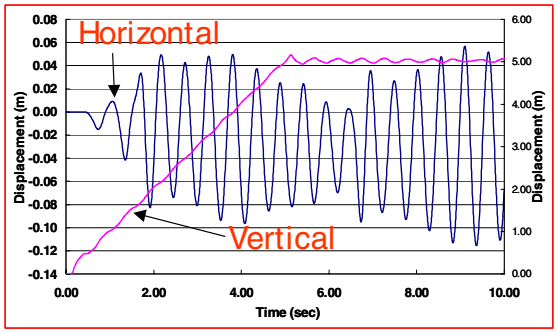

(a) Horizontal and vertical displacement time history (Haskell model)

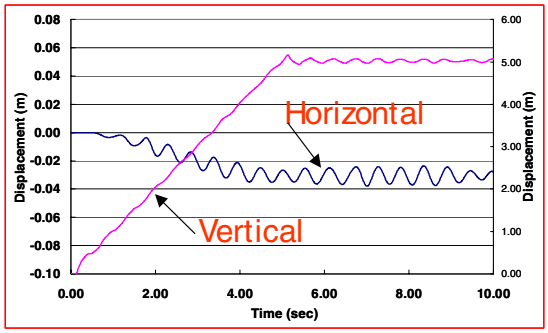

(a) Horizontal and vertical displacement time history (Cosine model)

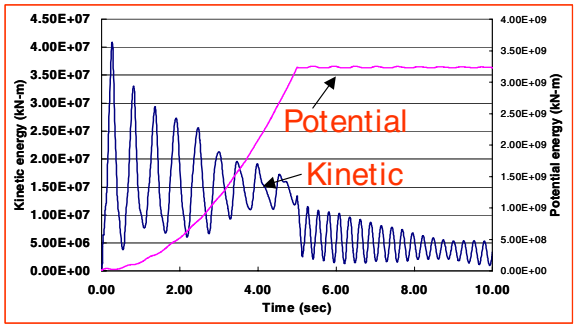

(b) Kinetic and potential energy changes in the system (Haskell model)

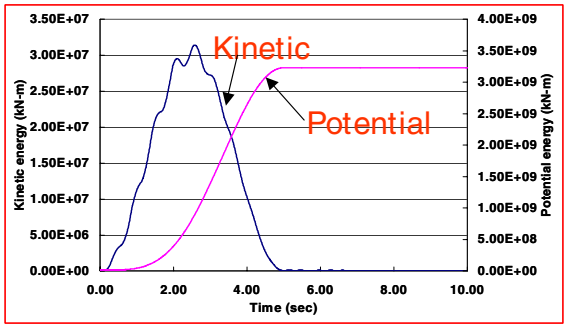

(b) Kinetic and potential energy changes in the system (Cosine model)

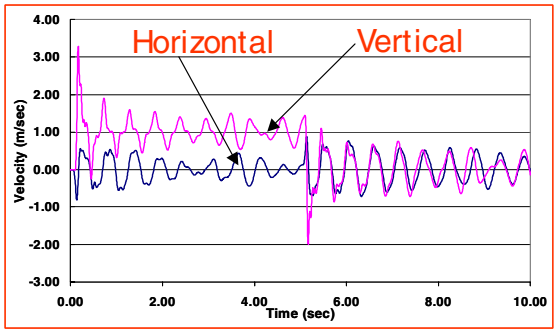

(c) Velocity time history of element "R5" on hanging wall (Haskell model)

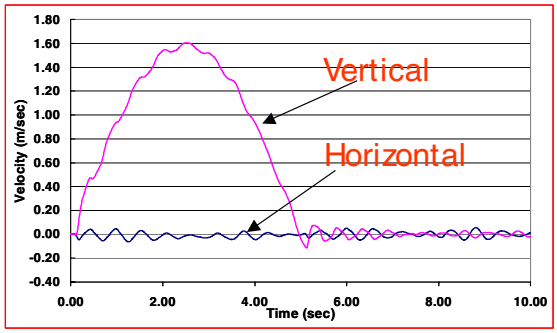

(c) Velocity time history of element "R5" on hanging wall (Cosine model)

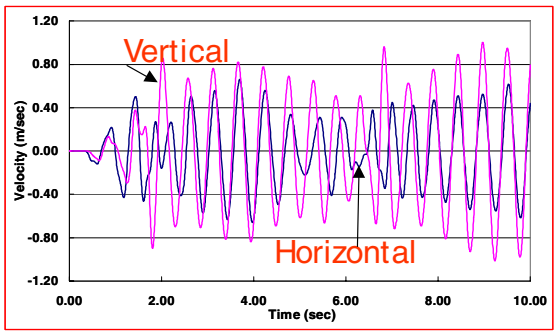

(d) Velocity time history of element "L5" on footwall (Haskell model)

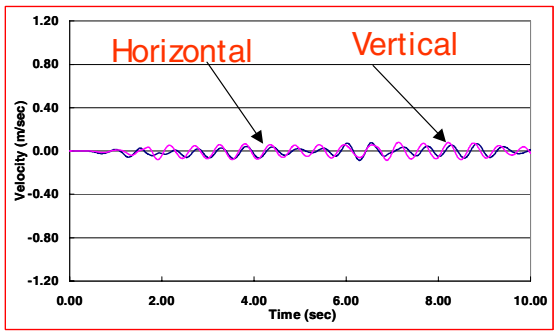

(d) Velocity time history of element "L5" on footwall (Cosine model)

Fig. 6 Effect of slip function on the response of soil deposit (case study using Haskell)

Fig. 7 Effect of slip function on the response of soil deposit (case study using Cosine model)

CASE STUDY

Permanent ground displacements that accompany a seismic event are the consequence of the fault slip and are referred as the static displacement field of that event or as coseismic displacements [14, 15]. This displacement field differs from the ground displacements induced by the seismic waves, which are generated during earthquakes rupture propagation and referred as dynamic displacement field. Despite their name, near–fault static displacements are developed rapidly, within short period of the time that is related to the slip rise time. The shortness of this development turns the coseismal displacement into a dynamic phenomenon. Since they are likely to be non-reversal and continuous, their time history will appear as a pulse of motion with a ramp-type shape. On observing the seismic records obtained during the Chi-chi earthquake [16]. It can be understood that the permanent relative ground displacement was responsible for most of the damage near the fault zone. For comparing the numerical analysis results with near field seismic records obtained during 1999, Chi-chi, Taiwan, a 2D microscopic model shown in **Fig. 4** is used. Response is measured at 6 observation points on the left and right side of the point exactly above the location of the underlying base fault. These points (L1 ~ L6 and R1 ~ R6) are located unevenly (i.e. at 5m, 25m, 65m, 145m, 305m, 485m) on each side.

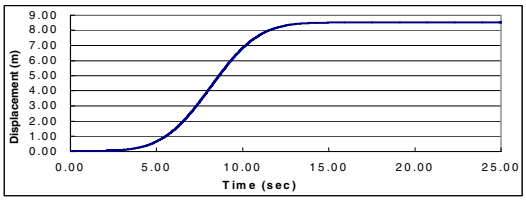

Fig. 8 Assumed static input displacement

For comparing the results with real near field records with large displacement, closed form approximation of static displacement is assumed. Pulse-like displacement time history that represents the base motion is considered (see **Fig. 8**) referring to Mladen [17]. As an approximation, the corresponding displacement pulse can be assumed as Gaussian-type function

$$d_{sp}(t) = \frac{\sqrt{2\pi}}{n} V_{sp} T_p \Phi\left[\frac{(t - t_c)}{T_p / n}\right] \qquad (4)$$

where V_{sp} is the amplitude of static velocity pulse, T_p Velocity pulse duration, t_c time instant, at which the pulse is centered, n constant equal to 6 and t is the time. The term T_p / n has the meaning of standard deviation and controls the actual spread of the pulse with respect to the given pulse duration and Φ is the normal probability function. For more details, please refer Mladen [17].

In general, the amplitude of wave attenuates because the material damping absorbs some of the elastic energy of the stress wave; the specific energy (energy per unit volume) decreases as the wave travels through a material. The reduction of specific energy causes the amplitude of the wave to decrease with distance. In purely elastic materials, the energy is conserved (no conversion to other forms of energy takes place), this reduction in amplitude due to spreading of the energy over a greater volume of material is often referred to as radiation damping (or geometric attenuation). It should be distinguished from material damping in which elastic energy is actually dissipated by viscous, hysteretic, or other mechanisms [18]. The above explanation says that the attenuation takes places from the shortest distance from the fault towards the farther distances. This is true when we discuss in large scale but when we look at the places very near to the fault trace, the scenario becomes different as will be explained below. Figures 9 (a) and (b) show the vertical and horizontal displacements respectively. From **Fig. 9 (a)** it can be seen that from R5 to R3, the displacement is same as the input displacement. However, from R3 to R2

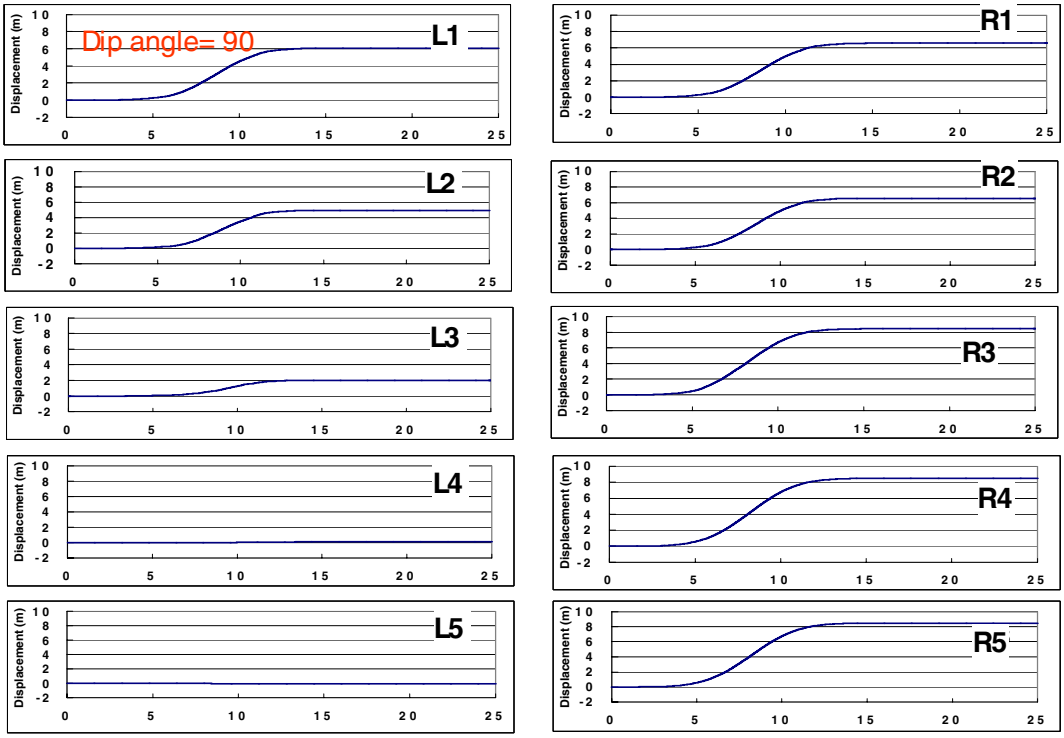

(a) Vertical surface displacement

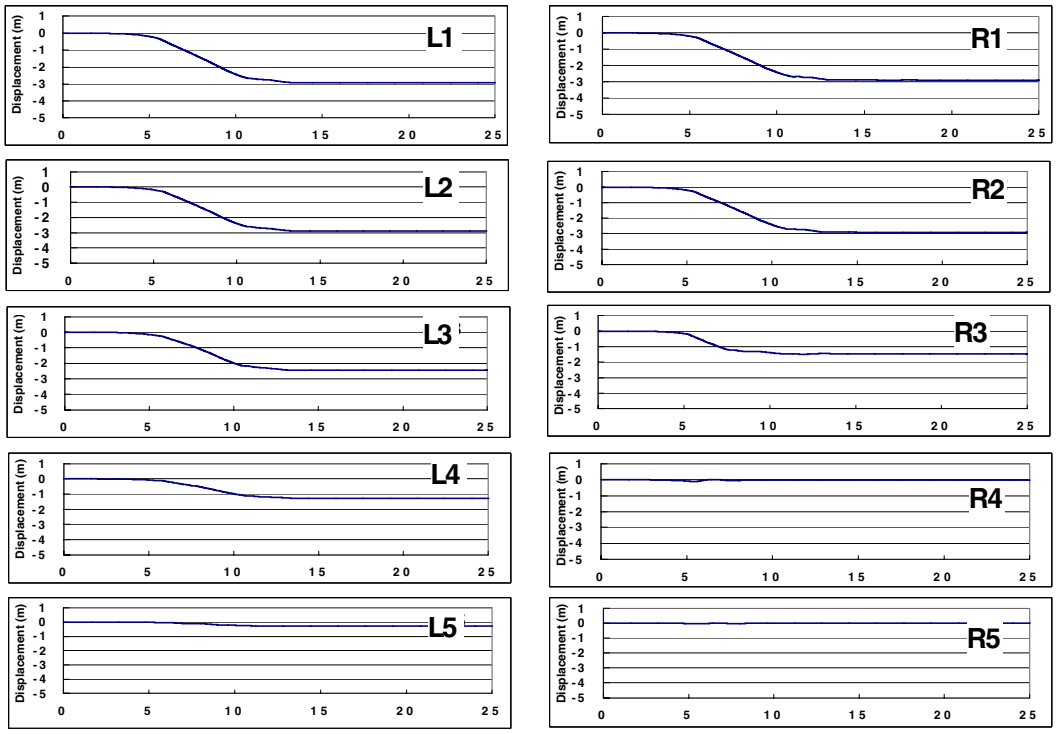

(b) Horizontal surface displacement

Fig. 9 Vertical and horizontal displacement time histories (at L1~L5 and R1~R5)

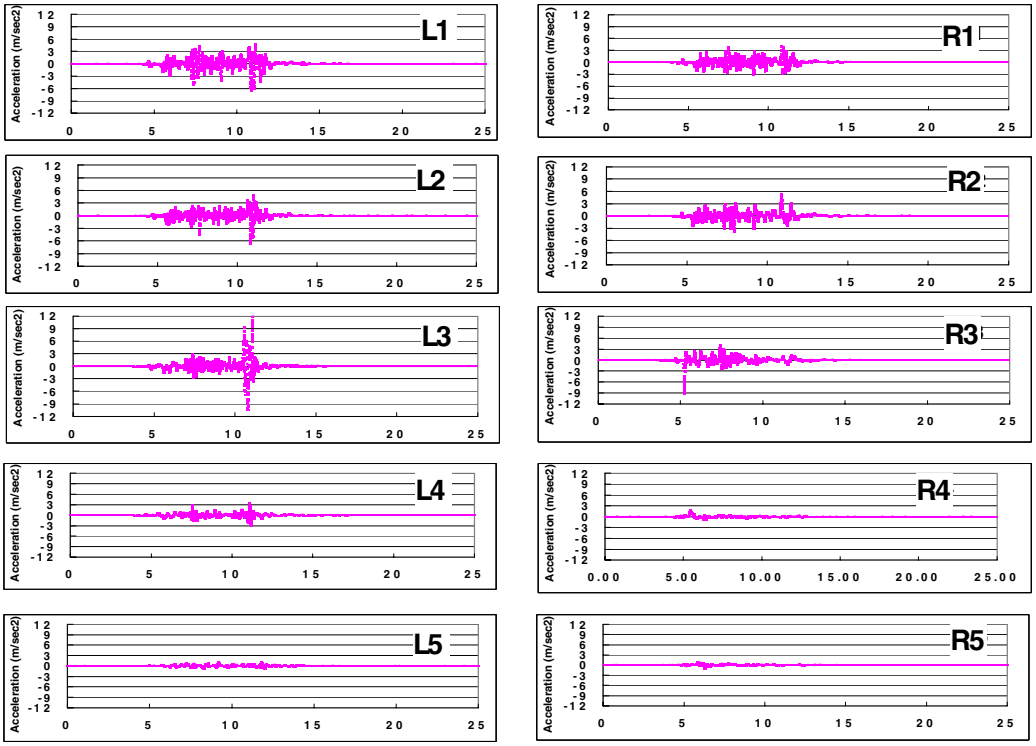

(a) Vertical acceleration time histories

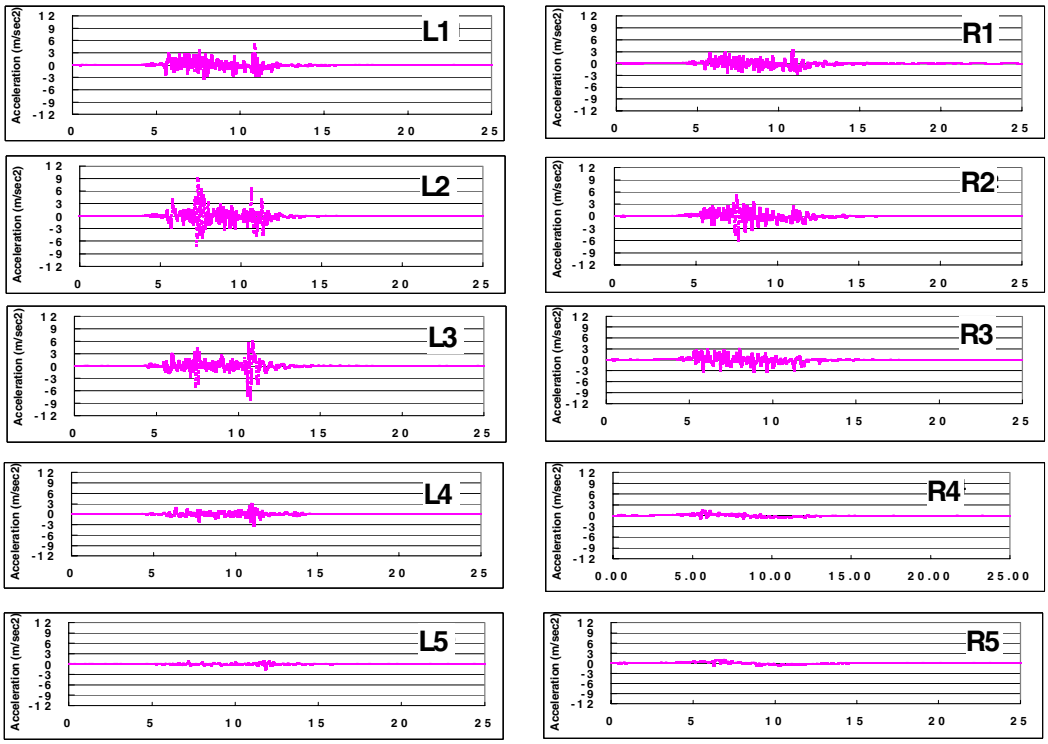

(b) Horizontal acceleration time histories

Fig.10 Vertical and horizontal acceleration time histories (at L1~L5 and R1~R5)

it decreases and finally it reaches to zero towards footwall side. From **Fig. 9 (b),** it can be seen that the effect of hanging wall displacement on the horizontal surface deformation is significant in the near fault region and towards the footwall. Figures 10 (a) and (b) show the vertical and horizontal acceleration time histories. It can be seen from this figure that the acceleration on surface attenuates when we move towards the farther distances due to failure from the fault. Spatial distribution of the final surface deformation in horizontal and vertical directions is shown in **Fig. 11**. Figure 12 (a) ~ (c) show the attenuation of peak ground acceleration, velocity and displacement respectively. Attenuation of peak ground acceleration (PGA) with respect to distance from the surface fault trace. It can be seen from the figure, that the PGA increases first and attains the peak value and then attenuates towards hanging wall direction. In general, the amount of destruction exactly on the fault is more because of the large relative permanent displacement. However, little away from the fault the damage is less because the amplitude of strong ground motion is not so high. And at farther distances, PGA attains greater magnitude and then decreases with distance. This phenomenon is sometimes observed during the past earthquakes. However, due to the sparse distribution of the seismometers, this could not be represented by actual recorded data. But with the help of the newly developed numerical model, we can show this phenomenon. The reason for this can be understood when we look at the propagation of cracks from the bedrock towards the surface (see **Fig. 13**). Near the surface fault rupture, the material becomes highly non-linear and the response of this region becomes low compared to the adjacent areas response.

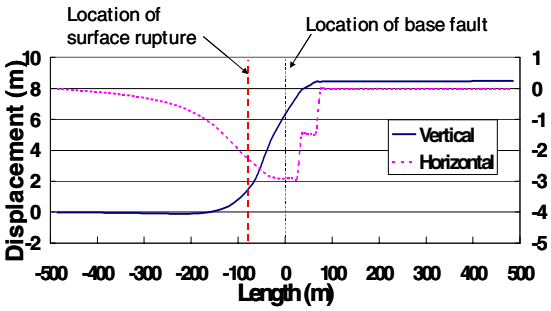

Fig. 11 Final surface displacement

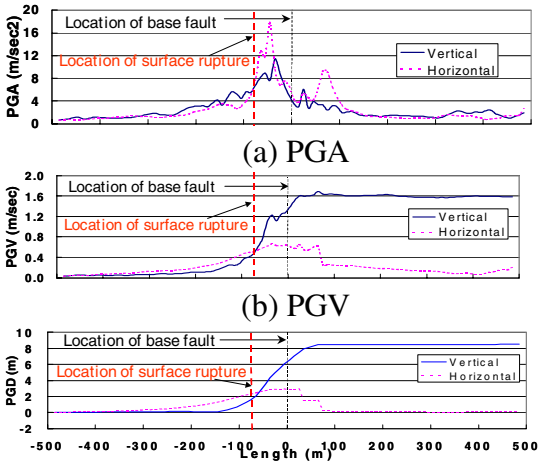

(a) PGA

(b) PGV

(c) PGD

Fig. 12 Attenuation of peak ground responses

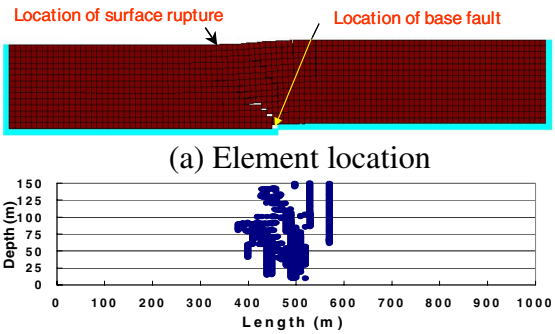

(a) Element location

(b) Crack propagation

Fig. 13 Element location and crack propagation responses

A complete understanding of the phenomenon of fault rupture propagation in soil may remain elusive because of the numerous governing factors that are highly variable and not well quantified. Geological observations of surface ruptures associated with historical earthquakes in the world have indicated that surface ruptures occurred, without any definite exceptions, on pre-existing faults. Moreover, there are lines of evidence indicating that moderate to large-scale faults have moved repeatedly in the geologic past. This is because a fault coalesces other faults and fractures near its edge every time it slips, and approaches to the ground surface with time. Conversely, a map-scale fault cannot be formed in a single event. The repetitive nature of faulting gives us an important basis for predicting future activity of faults

by using geologic information. And hence, the study on the fault rupture propagation is necessary to establish the possible locations of the faults appearing on the surface due to future earthquakes because engineers are more concerned about the damage that will be caused when the structures are located on the vulnerable area.

CONCLUSIONS

A new application to Applied Element Method (AEM) is proposed in this paper. Numerical modelling of fault rupture propagation in dynamic condition is done using 2D AEM. It is found from the results that the PGA very near to the fault trace becomes relatively smaller and increases to peak value and then attenuates towards the hanging wall side.

REFERENCES

1. Japan Society of Civil Engineers, *The 1999 Kocaeli earthquake, Turkey, Investigation into damage to civil engineering structures*, Earthquake Engineering Committee, Japan Society of Civil Engineers, 1999 (a).
2. Japan Society of Civil Engineers, The 1999 Ji-Ji earthquake, Taiwan, Investigation into damage to civil engineering structures, Earthquake Engineering Committee, Japan Society of Civil Engineers, 1999 (b).
3. Cole, D. A., Jr., and Lade, P. V., *Influence zones in alluvium over dip-slip faults*, Journal of Geotechnical Engineering, ASCE, Proc. Paper 18788, Vol. 110, No. GT5, pp. 599-615, 1984.
4. Lade, P. V., Cole, D. A., Jr., and Cummings David., *Multiple failure surfaces over dip-slip faults*, Journal of Geotechnical Engineering, ASCE, Proc. Paper 18789, Vol. 110, No. GT5, pp. 616-627, 1984.
5. Onizuka, N., Hakuno, M., Iwashita, K. and Suzuki, T., *Deformation in grounds and bedrock stress induced by reverse dip-slip faults*, Journal of Applied Mechanics, JSCE, Vol. 2, pp. 533-542, 1999 (in Japanese).
6. Bray, J.D., *The effects of tectonic movements on stresses and deformations in earth embankments*, Dissertation doctor of philosophy, University of California, Berkeley, 1990.
7. Tani, K., Ueta, K., and Onizuka, N.: *Scale effects of Quarternary Ground Deformation observed in Model Tests of vertical Fault*, Proceedings 29th Japan National Conference of Soil Mechanics and Foundation Engineering, pp. 1359-1562, 1994 (in Japanese).
8. Hakuno, M., Meguro, K.: *Simulation of concrete-frame collapse due to dynamic loading*, Journal of Engineering Mechanics, ASCE, Vol. 119, No. 9, September, 1993.
9. Meguro, K. and Tagel-Din, H., *Applied element method for structural analysis: Theory and application for linear materials*, Structural Eng./Earthquake Eng., JSCE, Vol. 17, No. 1, 21s-35s, 2000.
10. Tagel-Din, H., *A new efficient method for nonlinear, large deformation and collapse analysis of structures*, Ph.D. thesis, Civil Eng. Dept., The University of Tokyo, 1998.
11. Meguro, K. and Tagel-Din H., *A new efficient technique for fracture analysis of structures*, Bulletin of Earthquake Resistant Structure Research Center, Institute of Industrial Science, The University of Tokyo, No. 30, 1997.
12. Ben-Menahem, A., and M.N. Toksoz: *Source mechanism from spectra of long period surface waves*, Journal of Geophysical Research 68: 5207-5222, 1963.
13. Haskell, N.A. *Radiation pattern of surface waves from point sources in a multi-layered medium*, Bulletin of Seismological Society of America 54: 377-394, 1964.

14. Hall, J.F., Heaton, T.H., Halling, M.W. and Wald, D.J., *Near-source ground motion and its effects on flexible buildings*, "Earthquake Spectra, 11(4), 569-605, 1995.
15. Tatcher, W., *Geodetic measurement of active tectonic processes,*' Active tectonics (studies in geophysics) 155-163, National Academy Press, 1986.
16. Lee, W.H.K., T.C. Shin, K.W. Kuo, and K.C. Chen, *CWB free-field strong motion Data from the 921 Chi-Chi Earthquake: Volume 1. digital acceleration files on CD-ROM, pre-publication version (December 6, 1999)*, Seismology Center, Central weather bureau, Taipei, Taiwan, 1999.
17. Mladen V. K., *Utilization of strong motion parameters for earthquake damage assessment of grounds and structures*, A dissertation submitted to the department of civil engineering (Ph.D. Thesis), University of Tokyo, 2000.
18. Kramer, S.L., *Geotechnical earthquake engineering*, Prentice-hall inc. Upper saddle river, New Jersey, pp.180, 1996.